Available online at www.sciencedirect.com
ScienceDirect
Journal of Nuclear Materials 367–370 (2007) 269–275
journal of nuclear materials
www.elsevier.com/locate/jnucmat

Diffuse X-ray scattering measurements of point defects and clusters in iron ☆

R.E. Stoller [a,*], F.J. Walker [a], E.D. Specht [a], D.M. Nicholson [b], R.I. Barabash [a], P. Zschack [c], G.E. Ice [a]

[a] *Oak Ridge National Laboratory, Materials Science and Technology Division, MS-6138, P.O. Box 2008, Oak Ridge, TN 37831-6138, USA*
[b] *Oak Ridge National Laboratory, Computing and Computational Sciences Division, Oak Ridge, TN, USA*
[c] *Argonne National Laboratory, Advanced Photon Source, Argonne, IL, USA*

Abstract

The nature of residual damage from atomic displacement cascades in iron has been investigated by diffuse X-ray scattering. A single crystal iron sample was irradiated at ~60 °C in the High Flux Isotope Reactor at the Oak Ridge National Laboratory to a fluence of 1×10^{23} n/m^2 ($E > 0.1$ MeV), or ~0.01 dpa. Diffuse X-ray scattering measurements were carried out at the Advanced Photon Source at the Argonne National Laboratory on three specimens: unirradiated, as-irradiated, and irradiated and annealed for one hour at 450 °C (IA). The specimens were cooled to ~40 K to minimize thermal diffuse scattering. Subsequent measurements of the specimen lattice parameter were completed at ORNL. The diffuse scattering in the as-irradiated specimen was dominated by interstitial defect clusters exhibiting a tetragonal distortion consistent with a ⟨1 0 0⟩ type defect. Substantial recovery of this defect component was observed following the anneal at 450 °C. A lattice parameter increase was observed following irradiation, which is also consistent with a substantial population of interstitial type defects. A net lattice parameter decrease was observed in the IA specimen, indicating loss of the interstitial defects with a residual population of vacancy-type defects.

1. Introduction

In recent years, molecular dynamics (MD) simulations of high energy displacement cascades have provided a detailed picture of primary damage formation in irradiated materials [1–7]. An unanticipated observation in these studies was extensive formation of small interstitial clusters that exhibited very high mobility. Two primary stable interstitial configurations are observed in iron, ⟨1 1 0⟩ and ⟨1 1 1⟩ dumbbells [3,4]. Empirical interatomic potentials predict that the difference in the formation energy between these configurations is ~0.1 eV [1–7]. More recent *ab initio* simulations [9] find the ⟨1 1 0⟩ dumbbell configuration to be lower energy than the ⟨1 1 1⟩ dumbbell configuration, but with a much larger difference of 0.7 eV. There is also significant disagreement between model predictions of mobility. MD simulations find the ⟨1 1 1⟩ dumbbell

☆ Research sponsored by the Division of Materials Sciences and Engineering, US Department of Energy, under contract DE-AC05-00OR22725 with UT-Battelle, LLC.
* Corresponding author. Tel.: +1 865 576 7886; fax: +1 865 241 3650.
E-mail address: rkn@ornl.gov (R.E. Stoller).

0022-3115/$ - see front matter © 2007 Elsevier B.V. All rights reserved.
doi:10.1016/j.jnucmat.2007.03.019

migrates with a low activation energy of ~0.1 eV, whereas the ⟨1 1 0⟩ dumbbell is essentially immobile near room temperature. However, *ab initio* simulations [9] find a very small energy barrier of about 0.05 eV between the ⟨1 1 1⟩ and ⟨1 1 0⟩ configurations. This suggests that the ⟨1 1 1⟩ dumbbell is not stable and is unlikely to play a significant role in defect migration. In either case, ⟨1 1 0⟩ dumbbells are predicted to dominate.

An understanding of the nature and mobility of these small interstitial clusters is important for predicting microstructural evolution. For example, extensive in-cascade clustering and low cluster mobility would give rise to a high cluster density which would act as sinks for other mobile defects. Conversely, if the clusters are as mobile as they appear in the MD simulations, the defect concentrations would be relatively low since they would easily migrate to fixed sinks such as dislocations and grain boundaries [8]. Similarly, the higher mobility of ⟨1 1 1⟩ defects implies that only the ⟨1 1 0⟩ type should be observed following irradiation. Further, although it is well established that by transmission electron microscopy (TEM) that interstitial loops of both ⟨1 0 0⟩ and ⟨1 1 1⟩ type are observed in iron following neutron and heavy ion irradiation [10,11] the mechanism by which the ⟨1 0 0⟩ loops form is not understood.

During the past two decades, the brilliance of the best X-ray sources has been doubling about every nine months. Recent progress in X-ray optics and commissioning of ultra brilliant third-generation synchrotron X-ray sources now allows for intense X-ray beams with 0.1–100 μm diameter spot size. These intense small beams enable experiments that were previously possible only with large single crystals. Previous X-ray analyses of irradiation-induced point defects, defect clusters, and dislocation loops are described in a number of papers [12–20], although studies in iron are not frequent. Small angle scattering [17] and measurements of electrical resistivity [18] have been used for the analysis of radiation induced defects in iron. Small angle scattering is sensitive to variations in scattering-length density but is not sensitive to local distortions. Since interstitial defects in iron cause strong lattice distortions in the surrounding matrix, diffuse X-ray scattering has been applied to their investigation [20]. The purpose of this work is to use X-ray scattering to investigate the residual damage from a low-dose, low-temperature irradiation of single crystal iron, and to compare the experimental observations with simulated scattering patterns to determine which type of interstitial defect cluster is formed. Lattice parameter measurements and the predictions of a kinetic radiation damage model are also used in the analysis.

2. Experimental: material and irradiation conditions

The material to be irradiated was obtained in the form of 0.999 + purity iron single crystal from Goodfellow Corporation. The disk-shaped sample was 2 mm thick and 1 cm in diameter; with a ⟨1 0 0⟩ specimen surface normal to the circular face. The as-received sample was sliced to provide two ~0.9 mm thick disk specimens. One of these specimens was irradiated at ~60 °C in a 'hydraulic tube' that passes through the core region of the High Flux Isotope Reactor (HFIR) at the Oak Ridge National Laboratory. The fast ($E > 0.1$ MeV) neutron flux in the HFIR axial location used is 8.9×10^{14} n/m^2/s. The exposure time was 3.12 h leading to a fast fluence of 1×10^{23} n/m^2, which corresponds to a dose of ~0.01 dpa in iron. Following the irradiation, the disk was cut in half and one of the disk halves was annealed at 450 °C for 1 h. Subsequent measurements were carried out on the single crystal iron in three conditions: as-received (AR), as-irradiated (AI), and post-irradiation annealed (PIA).

3. Diffuse X-Ray scattering measurements and scattering simulations

Diffuse X-ray scattering measurements were carried out at the Advanced Photon Source (APS) at the Argonne National Laboratory. A custom aluminum holder was designed and built for the radioactive AI and PIA specimens to avoid contaminating APS equipment while permitting cryogenic examination. Measurements were carried out in the APS UNICAT beam lines 33BM and 33ID with a beam energy of 20 keV. The small beam spot size obtained in this facility, ~50 μm × 50 μm, permits essentially single-grain measurements even in polycrystalline samples. The effective beam size was larger for these irradiated single crystal specimens, 1 mm × 2 mm, due to the geometry and constraints imposed by the specimen holder. An energy dispersive detector was employed to measure the Compton scattering to aid in background subtraction and calibrate the incident beam intensity.

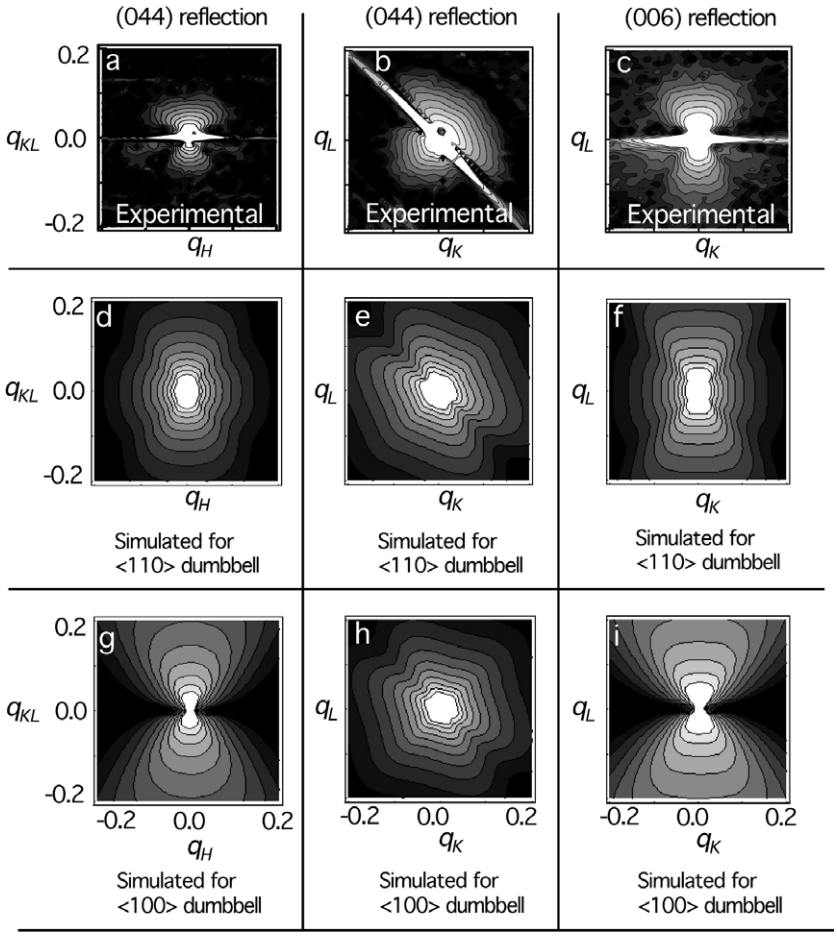

Fig. 1. Diffuse scattering measurements and Huang scattering comparison. Panels a–c are log plots of measurements of diffuse scattering intensity. Panels d–i plot the log intensity for the two dumbbell configurations for comparison to the measured scattering.

The diffuse scattering measurements shown in Fig. 1(a)–(c) were obtained by subtracting the measured intensity from the AI sample from the PIA sample. The AR sample data could not be used as the basis for this subtraction because it was not obtained in the aluminum holder. The intense scattering seen as a bright streak perpendicular to the radial direction in reciprocal space is an artifact of the differing crystal mosaics present in the two different pieces of iron. The higher measured intensity for scattering vectors larger than the Bragg peak is dominated by diffuse scattering from interstitial defect clusters, while scattering at smaller scattering vectors has contributions from both interstitial and vacancy type defect clusters. The shape of the scattering can be used to determine the symmetry of the scattering defect.

Analysis was focused on the shape of the diffuse intensity on the high q side of the Bragg reflection and Huang scattering from $\langle 1\,1\,0\rangle$ interstitial dumbbells and $\langle 1\,0\,0\rangle$ interstitial dumbbells was simulated. The scattered intensity was modeled by an elastic dipole in the iron lattice due to a $\langle 1\,1\,0\rangle$ split interstitial. The dipole is specified by the tensor P

$$P = \begin{pmatrix} 14 & 9 & 0 \\ 9 & 14 & 0 \\ 0 & 0 & 19 \end{pmatrix} \text{eV}. \quad (1)$$

This dipole tensor was deduced by Peisl, et al. [20] for isolated point defects in electron irradiated iron. The shape of the measured scattering does not match simulations of $\langle 1\,1\,0\rangle$ dumbbells. Simulations of the scattering for a dipole force tensor without the off-diagonal terms, consistent with a $\langle 1\,0\,0\rangle$ defect symmetry provides a better match.

This conclusion is problematic because the $\langle 1\,0\,0\rangle$ interstitial dumbbell configuration is unstable in bcc

iron relative to either the ⟨1 1 0⟩ or ⟨1 1 1⟩ dumbbell. It is possible that clustering of interstitials stabilizes the ⟨1 0 0⟩ configuration of the individual interstitials. An alternate explanation lies in the stabilization of defect clusters with tetragonal symmetry. However, the results of the MD simulations indicate that the interstitial directions align regardless of the individual point defect symmetry. Therefore, it appears that the symmetry of the interstitial is the symmetry of the cluster, and this symmetry is ⟨1 0 0⟩.

The effect of the one-hour post-irradiation anneal at 450 °C is shown in Fig. 2, where the measured diffracted intensity around the 0 0 6 reflection is shown for the irradiated specimen in (a) and for the post-irradiation annealed specimen in (b). The loss of intensity at large scattering vectors perpendicular to the mosaic streak provides clear evidence of defect recovery. An estimate of the size of the scattering feature can be obtained from Fig. 3 which plots the scattered intensity as a function of the scattering vector q in reciprocal lattice units. The crossover from Huang scattering ($I \sim 1/q^2$) to Stokes–Wilson scattering ($I \sim 1/q^4$) observed at ~0.7 rlu, corresponds to a real space length of ~1.4 nm for the radius of the heavily distorted lattice around the defect cluster [21]. If this corresponds to the extent of the interstitial distribution within the cluster the containing a close-packed array of ⟨1 0 0⟩ dumbbells, it would accommodate 15–20 interstitials. However, the actual size of the cluster must be smaller than the highly-strained volume as was the case in the study by Peisl et al. [19] where they observed four interstitials per cluster. MD calculations of lattice displacements near point clusters were carried out to permit numerical simulation of the scattering from interstitial and vacancy configurations [14] in an attempt to match the observed scattering (Fig. 3).

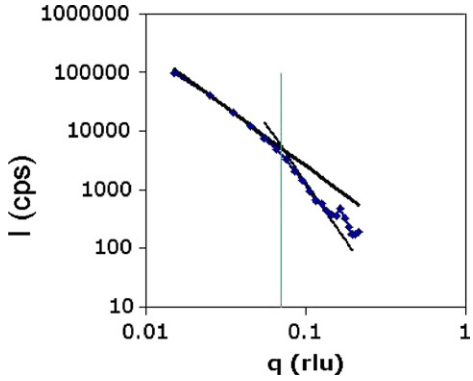

Fig. 3. Diffracted intensity as a function of q in reciprocal lattice units. Slope change at ~0.65 nm corresponds to radius of strained volume (larger than physical size of interstitial cluster).

Defect configurations for additional scattering simulations were prepared by molecular dynamics using the Moldy code and a modified version of the Finnis–Sinclair interatomic potential [1]. Configurations of small interstitial clusters composed of up to 15⟨1 0 0⟩, ⟨1 1 0⟩, or ⟨1 1 1⟩ were relaxed and quenched in cells of 16,000 atoms. The MD cluster configurations were used to construct larger cells with 128,000 atoms for simulation of X-ray scattering. Each MD structure was described in terms of vacancies and interstitial coordinates relative to

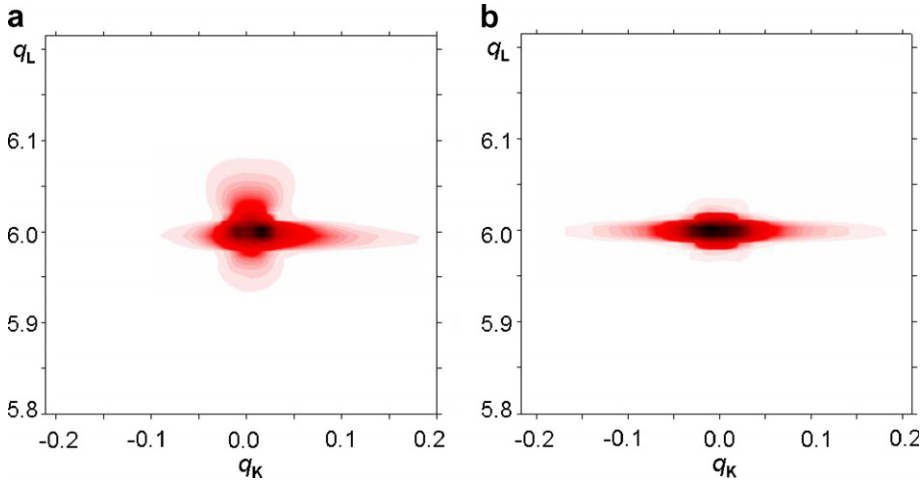

Fig. 2. Effect of one-hour post-irradiation anneal at 450 °C on diffuse scattering intensity (Log scale) near 006 reflection in (0, K, L) plane. Loss of scattering intensity indicates defect recovery.

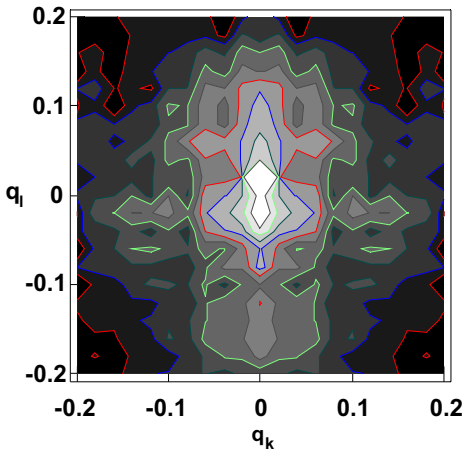

Fig. 4. Simulated diffuse scattering pattern for ⟨100⟩ interstitial cluster containing nine dumbbells. Logarithm of intensity around 006 reflection, q in reciprocal lattice units.

the center of the cluster, and the displacements of the remaining atoms. Equivalent configurations result from lattice translations and application of the 48 cubic rotations. Configurations were selected by randomly choosing translation/rotation pairs and were applied in the larger cell by removing vacancies, adding interstitials and accumulating atomic displacements while preventing clusters from overlapping one other. Coherent scattering was calculated directly and the resulting intensity was symmetrized. Diffuse scattering maps were calculated for the most likely interstitial clusters containing different numbers of dumbbells, including ⟨110⟩, ⟨111⟩, ⟨100⟩. Details of the diffuse scattering simulations and examples of reciprocal space maps through different planes of reciprocal space caused by these configurations can be found in the Ref. [22]. Diffuse intensity distributions are distinct for the different defects configurations. An example of the simulated scattering intensity around a 006 reflection is shown in Fig. 4 for a 9-dumbbell, ⟨100⟩ cluster. This result is consistent with the measured results shown in Figs. 1(c) and 2(a).

4. Lattice parameter measurements

Additional measurements of specimen lattice parameter were carried out at ORNL. Lattice parameters were measured at room temperature using a high-precision triple-axis technique with a rotating anode source (50 kV, 100 mA) providing Cu radiation. Si(111) crystals placed before and after the sample collimated the incident and diffracted beams. A slit between the first crystal and the sample selected Cu $K_{\alpha 1}$. The sample was oriented using a four-circle diffractometer. Lattice parameters were calculated from $\theta/2\theta$ scans of the Fe(211) reflections; the peak positions were found from a using least-squares fit to a Gaussian line shape. The diffractometer 2θ value was calibrated using a Si(004) reflection ($a_0 = 0.54308$ nm). Lattice parameter measurements for the three specimens are given in Table 1.

Table 1
Results of lattice parameter measurements on single crystal iron

Specimen condition	Lattice parameter, a_0 (nm)	Lattice parameter change, $\Delta a/a_0$
Unirradiated	0.28666	n/a
As-irradiated	0.28668	7.0×10^{-5}
Post-irradiation annealed	0.28664	-8.0×10^{-5}

The relaxation volume (Ω) of an interstitial is of opposite sign, and more than an order of magnitude larger than that of a vacancy: $\Omega_i \sim 1.2\,\Omega_0$ and $\Omega_v \sim -0.05\,\Omega_0$, where Ω_0 is the atomic volume [23]. Thus, the lattice parameter increase due to the irradiation indicates that a substantial number of interstitial-type defects are present. Although the irradiation creates equal numbers of vacancies and interstitials, some fraction of the mobile point defects are expected to be lost to sinks during irradiation at ~60 °C. Based on the difference between the vacancy and interstitial migration energies, one would expect that more vacancies would survive than interstitials. However, the larger interstitial relaxation volume could still cause a net increase in lattice parameter. A reasonable lower limit estimate of the interstitials present (N_i) can be obtained if one assumes that an equal number of vacancies (N_v) and interstitials have survived. Applying the value of $1.2\,\Omega_0$ for the relaxation volume of a Frenkel pair [23], and the relationship [24]

$$3\frac{\Delta a}{a_0} = \Omega_i N_i + \Omega_v N_v = \Omega_{FP} N_{i,v}, \qquad (2)$$

the number of point defects would be $\sim 1.8 \times 10^{-4}$ per atom. Note that N_i and N_v refer to the sum of all surviving defects, including those in clusters. A simulation of the irradiation using the kinetic model and parameters discussed in Ref. [8] leads to a calculated total concentration of interstitial defects of 1.2×10^{-4} per atom.

Consistent with the change in scattering, the lattice parameter change following the anneal indicates substantial loss of the diffuse scattering interstitial defects. The negative lattice parameter change indicates that the majority of defects that survive the annealing must be vacancy type. A lower limit on the number of vacancy defects can be obtained by assuming that all the interstitial defects have been annealed. Applying $\Omega_v = -0.05\,\Omega_0$ and $N_i = 0$ in Eq. (2) leads to a concentration of 4.8×10^{-3} per atom. The same simulation mentioned above results in a total surviving vacancy population of 1.2×10^{-3} per atom. The calculated values of N_i and N_v are sensitive to parameters such as their migration energies and the displacement cascade survival efficiency; plausible variations in these parameters can cause N_i and N_v to change by more than one order of magnitude. Thus, the values of N_i and N_v inferred from the lattice parameter change measurements appear to be in reasonable agreement with model predictions.

5. Discussion and summary

The results obtained to date indicate that a substantial fraction of the interstitials created in displacement cascades survive in the form of small $\langle 1\,0\,0\rangle$ clusters that are stable at well above room temperature. This suggests that interstitial cluster formation and evolution may be more complex than indicated by the results obtained in MD simulations employing embedded atom type interatomic potentials. Reasonable agreement was obtained with a kinetic simulation in which no highly mobile $\langle 1\,1\,1\rangle$-type clusters were assumed to form. The thermal stability of the interstitial clusters can only be roughly estimated from the annealing results. Essentially full recovery occurred during a one-hour anneal at 450 °C, while the results indicate that little or no recovery occurred during the 16 month period the specimens were at room temperature between the irradiation and examination at APS. Assuming that the recovery is controlled by diffusion and the process can be characterized by a diffusion length proportional to the square root of the product of the diffusion coefficient and time, the activation energy for the process would be between 0.6 and 0.8 eV to obtain 10 to 100 times more recovery during the anneal than during storage. This value is much higher than that expected for small interstitial cluster migration, but is consistent with vacancy migration in pure iron, implying that vacancies are diffusing and recombining with the interstitial defects. However, this mechanism would require a very high initial concentration of vacancy-type defects because the lattice parameter measurements indicate that a large population remains after the anneal.

It is clear that additional scattering measurements and analysis are required to confirm the results obtained in this study. Ideally, cryogenic irradiation to lower doses and cryogenic storage should be used to eliminate any defect migration and recovery prior to examination. A continuous *in situ* annealing and measurement capability would also improve the reliability of the data. Currently, more detailed simulations of diffuse scattering are underway to improve the quality of the comparison between experimental measurements and simulations, and to provide guidance for future experiments. Modern synchrotron X-ray sources with high intensity and small spot sizes provide a new opportunity to exploit diffuse scattering measurements as a nondestructive tool to characterize primary damage formation in irradiated materials.

Acknowledgements

Research sponsored by the Division of Materials Sciences and Engineering, US Department of Energy under contract DE-AC05-00OR22725 with UT-Battelle, LLC.

References

[1] R.E. Stoller, A.F. Calder, J. Nucl. Mater. 283–287 (2000) 746.
[2] W.J. Phythian, R.E. Stoller, A.J.E. Foreman, A.F. Calder, D.J. Bacon, J. Nucl. Mater. 223 (1995) 245.
[3] R.E. Stoller, G.R. Odette, B.D. Wirth, J. Nucl. Mater. 251 (1997) 49.
[4] R.E. Stoller, J. Nucl. Mater. 276 (2000) 22.
[5] D.J. Bacon, F. Gao, Yu.N. Osetsky, J. Nucl. Mater. 276 (2000) 1.
[6] M.J. Caturla, N. Soneda, E. Alonso, B.D. Wirth, T. Diaz de la Rubia, J.M. Perlado, J. Nucl. Mater. 276 (2000) 13.
[7] K. Nordlund, R.S. Averback, J. Nucl. Mater. 276 (2000) 194.
[8] R.E. Stoller, in: R.K. Nanstad, M.L. Hamilton, F.A. Garner, A.S. Kumar (Eds.), Effects of Radiation on Materials, ASTM STP 1325, ASTM International, West Conshohocken, PA, 1999, p. 15.
[9] Chu-Chun Fu, F. Willaime, P. Ordejon, PRL 92 (2004) 175503.
[10] I.M. Robertson, M.L. Jenkins, C.A. English, J. Nucl. Mater. 108&109 (1982) 209.
[11] L.L. Horton, J. Bentley, W.A. Jesser, J. Nucl. Mater. 103&104 (1981) 1085.

[12] H.G. Haubold, Revue de Physique Appliquee 11 (1976) 73.
[13] B.C. Larson, J. Appl. Cryst. 8 (1975) 150.
[14] B.C. Larson, F.W. Young Jr., Phys. Stat. Sol. A 104 (1987) 273.
[15] B.C. Larson, W. Schmatz, Phys. Stat. Sol. B 99 (1980) 267.
[16] B. Schonfeld, P. Ehrhart, Phys. Rev. B. 19 (1979) 3905.
[17] H. Franz, G. Wallner, J. Peisl, Radiat. Eff. Def. Solids 128 (1994) 189.
[18] H. Abe, E. Kuramoto, J. Nucl. Mater. 283–287 (2000) 174.
[19] H. Peisl, J. Appl. Cryst. 8 (1975) 143.
[20] J. Peisl, H. Franz, A. Schmalzbauer, G. Wallner, in: P.D. Bristowe, J.E. Epperson, J.E. Griffith, Z. Liliental-Weber (Eds.), Defects in Metals, MRS Vol. 209, MRS, Warrendale, PA, 1991, p. 271.
[21] P.H. Dederichs, J. Phys. F: Met. Phys. 3 (1973) 471.
[22] R.E. Stoller, G.E. Ice, R.I. Barabash, in: R. Finch, D. Bullen (Eds.), II Scientific Basis for Nuclear Waste Management, Mat. Res. Soc., vol. 757, Warrendale, PA, 2003, p. II413.1.
[23] P. Ehrhart, in: H. Ullmaier (Ed.), Atomic Defects in Metals, Group III: Crystal and Solid State Physics, New Series, Springer-Verlag, Berlin, 1991.
[24] R.O. Simmons, R.W. Balluffi, J. Appl. Phys. 30 (1959) 1249.